Progress In Electromagnetics Research, PIER 94, 175–195, 2009

LAYER-MODE TRANSPARENT BOUNDARY CONDITION FOR THE HYBRID FD-FD METHOD

H.-W. Chang, W.-C. Cheng, and S.-M. Lu

Institute of Electro-optical Engineering and Department of Photonics
National Sun Yat-sen University
Kaohsiung 80424, Taiwan

Abstract—We combine the analytic eigen mode expansion method with the finite-difference, frequency-domain (FD-FD) method to study two-dimensional (2-D) optical waveguide devices for both TE and TM polarizations. For this we develop a layer-mode based transparent boundary condition (LM-TBC) to assist launching of an arbitrary incident wave field and to direct the reflected and the transmitted scattered wave fields back and forward to the analytical regions. LM-TBC is capable of transmitting all modes including guiding modes, cladding modes and even evanescent waves leaving the FD domain. Both TE and TM results are compared and verified with exact free space Green's function and a semi-analytical solution.

1. INTRODUCTION

Passive dielectric waveguides devices are important building blocks in modern optical communication systems [1, 2]. For 2-D dielectric waveguide problems are divided into mutually independent TE and TM cases which can be solved as scalar wave problems [3, 4]. For complex optical devices, full wave methods such as the finite-difference time-domain methods (FD-TD) [5–7] are often used. For very large adiabatic waveguide devices the beam propagation method (BPM) and its variations [8] are used for studying field evolutions and for mode profile determination. BPMs apply a one-way approximation to the Maxwell's equations making it possible to advance the field solutions plane by plane along the propagation axis. This tremendous saving in computational resources makes BPM the only available option for modeling large complex 3D waveguide devices.

Corresponding author: H.-W. Chang (hchang@faculty.nsysu.edu.tw).

In 1966 Professor Yee published his now famous 3D FD-TD algorithm [9]. It was until 1975 when workstations became popular and powerful enough that Taflove and Brodwin, based on Yee's time stepping algorithm, published a few 2-D and 3D microwave simulation papers [10, 11]. Holland, Kunz and Lee applied Yee's method and published several EMP paper in 1977 [12, 13]. Since then, FD-TD had gained popularity as one viable method for many EM problems.

To keep the FD-TD domain from becoming too large, various absorbing/transparent boundary conditions (ABC/TBC) were developed to allow scattered wave fields to leave the FD-TD region. There are basically two types of ABC/TBC [14]. The first group is based on the one-way wave equation such as Mur ABC [15]. The method is simple but is only effective for waves with small incident angles. Lindman [16] extended it to wider incident angles using a much more complex formulae. Liao, et al. [17] extended the TBC to handle waves in horizontally stratified media with multiple wave types. Several ABC modifications and extensions were also published for acoustical and seismic applications. Examples include Grote's nonreflecting BC (NBC) [18], Engquist's method [19, 20]. In 1992 Hadley published a first BPM TBC paper [21] based on a first-order linear phase extrapolation method.

The second ABC/TBC group is based on absorbing materials. Berenger published two papers on perfectly matched layer, PML [22–24] which became very popular for ease of use and for its effectiveness. PML methods require that part of FD region near the boundaries to be padded with electric and magnetic absorbing materials. The impedance of PML material is chosen to be the same as the background material (for the normally incident waves) to reduce the reflection. However, waves coming in at near grazing angles will be reflected due to larger mismatch in the wave impedance. By optimizing PML parameters zero reflection can be obtained for isolated pairs of frequency and angle of incidence [25].

Both types of ABC/TBC methods are designed for absorbing waves in homogeneous media. The performance of the FD-TD ABC methods will be degraded for optical waveguide devices with horizontally stratified media with discrete material indices [26]. To overcome this difficulty, there are currently ongoing research efforts on applying PML/ABC for layered media [27]. In addition, the characteristic of an optical waveguide device is completely determined by the dispersion relation at the optical carrier frequency. Frequency-domain analysis allows us to study waveguide physics easier than the time-domain method. For example, to obtain the group velocity and group delay of a given waveguide device, we need a very high frequency resolution near the carrier frequency. High frequency resolution from

FD-TD simulation requires a very long run time. Since late arriving signals are bouncing between ABC regions, a high-quality long run time FD-TD calculation requires a very good ABC/TBC especially in a layered dielectric structure. Thus, we seek for a good ABC/TBC method for FD-FD method, which has recently become quite popular for modeling some complex optical device [28, 29].

The disadvantage of the FD-FD method is that we need to solve for a large linear equation of up to a few million variables. As far as we know there exists no robust and fast iterative method, such as the ADI method for the Laplace equation, for solving the discretized Helmholtz equation. In fact, FD-TD can be considered as a special iterative method for solving FD-FD matrix equation with simple boundary conditions. In general FD-FD method is more accurate than the FD-TD method, since there is no approximation of the time-derivative operator. The lack of robust iterative discretized Helmholtz solver is the limiting factor for all FD-FD applications. As a result, all practical FD-FD simulations are 2-D. And it should be treated as the supplemental to the FD-TD method.

To take the advantages of analytical methods in the frequency domain, we combine FD-FD method, which is good for complex structures, with eigen mode expansion techniques, which are better suited for the input and output regions made of a waveguide structure. The hybrid approaches possess the strengths and efficiency of each numerical technique [30]. To connect the FD-FD region with the two analytical regions, we developed a layer-mode based transparent boundary condition to assist launching of an arbitrary incident wave field, and in the same time, to direct the reflected and the transmitted scattered wave fields back to the analytical regions. The initial work was published first by author's student as a master thesis [31] and later on, as an application paper [32]. Part of the material in this paper was explained in a conference paper [33] where we did a comparison with the FD-FD using PML as the transparent boundary. LM-TBC is based on one-way Helmholtz equation and thus requires no additional padding regions like the PML. It is designed for transmitting multiple outgoing waves in a multi-layer medium while simultaneously allows an arbitrary incident field to enter the FD region.

2. THEORETICAL FORMULATION FOR LM-TBC

2.1. The Hybrid FD-FD Method

Figure 1 illustrates the application of the hybrid FD-FD to the study of a quasi-adiabatic tapered waveguide device that connects a 7 µm-thick input waveguide to 3 µm-thick output waveguide. This tapered

waveguide device operates at a wavelength $\lambda = 1.3\,\mu\text{m}$ has a glass core (index = 1.5) surrounded in the air (cladding index = 1). The problem domain is horizontally divided into three regions. Region I and III are the input and output region made of a horizontal slab waveguide. The two waveguide are connected by a linearly tapered waveguide in Region II. The core-cladding boundary is indicated by the blue lines.

Optical waveguide designers are interested in designing a compact taper structure to ensure a smooth transition between the fundamental input waveguide mode and the fundamental output waveguide mode. Power loss due to radiation and higher-order mode conversion should be kept to a minimum. We see clearly from our hybrid FD-FD simulation that this tapered waveguide with a 15° taper angle converts most the input energy into the output waveguide but also excites quite a lot higher order mode power.

Note that field in Regions I and III is computed analytically while field in Region II is computed by solving the FD-FD matrix equation. It is known that tangential electric field component and it normal derivative are continuous everywhere in a piece-wise constant dielectric waveguide device. Careful inspection of the field component $E_y(x, z)$ of Figure 1 reveals a continuous and smooth transition across core-cladding interfaces and over the two computational boundaries. There are no noticeable numerical artifacts. Our proposed LM-TBC has successfully launched the incident field into the FD-FD region and transmitted multiple waveguide mode fields to the exit waveguide.

For simplicity we assume that a general 2D waveguide device is embedded in a parallel-plate structure. It is horizontally divided into three regions with the FD-FD region sandwiched between two analytical regions. For this hybrid FD-FD method to work, the multi-layer structure in the input and the output region must be aligned with the z-axis. To understand how we combine the three regions into one self-consistent FD-FD formulation let us refer to Figure 2 where we show the layout of FD-FD grids. The unknowns are the FD-FD variables in Region II. The center of the coordinate $(0, 0)$ is assumed to located at the lower left corner of the FD-FD region. The central field component is $E_y(x, z)$ for TE polarization and $H_y(x, z)$ for TM. In FD region the field $u^{\text{II}}(x, z)$ is uniformly sampled into a rectangular array of discrete points $\{u_{i,j}\}$, where $u_{i,j} = u^{\text{II}}(x_i, z_j)$. We shall group them into M column vectors each with a length N so that

$$\mathbf{u}_j = \begin{bmatrix} u_{1,j} \\ \vdots \\ u_{N,j} \end{bmatrix}, \quad j = 1, \ldots, M, \tag{1a}$$

where

$$u_{i,j} = u(x_i, z_j), \quad x_i = (i - 1/2)\,\Delta x, \quad z_j = (j - 1)\,\Delta z. \tag{1b}$$

Note that $\mathbf{u}_1$ vector is chosen to be on the interface between Region I and Region II at $z = 0$. Similarly $\mathbf{u}_M$ vector is chosen to be on the interface between Region II and Region III at $z = L_z$.

The field in Region I, the input analytical region, is made of the incident wave and the reflected waves reflected off the FD-FD region as

$$u^{\mathrm{I}}(x, z) = \phi_1^{\mathrm{I}}(x) e^{-j\beta_1^{\mathrm{I}} z} + \sum_{n=1}^{N} r'_n \phi_n^{\mathrm{I}}(x) e^{j\beta_n^{\mathrm{I}} z}, \quad z \le 0 \tag{2}$$

where $\phi_n^{\mathrm{I}}(x)$ and β_n^{I} is the nth eigenmode and corresponding propagation constant of the input waveguide, and r'_n is the nth reflection coefficient. The incident wave is immediately combined with a reflected wave to form a standing wave so that the net contribution of the "incident" field at the Region I–II interface is zero. Thus we

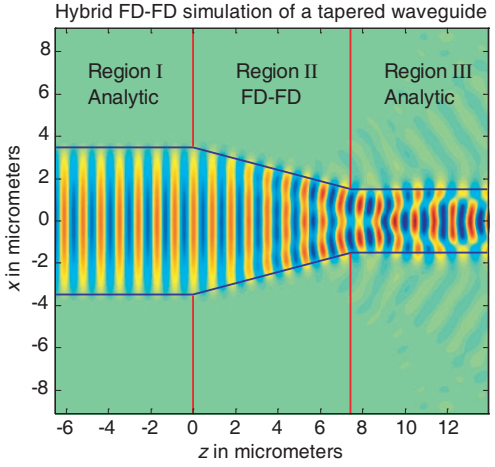

Figure 1. Illustration of the hybrid FD-FD method applied to a quasi-adiabatic tapered waveguide device. The field $E_y(x, z)$ is excited by A TE-polarized fundamental mode incident wave. This ideal 2-D device is made of a glass core with an air cladding.

have

$$u^{\mathrm{I}}(x,z) = -2j\phi_1^{\mathrm{I}}(x)\sin(\beta_1^{\mathrm{I}} z) + \sum_{n=1}^{N} r_n \phi_n^{\mathrm{I}}(x) e^{j\beta_n^{\mathrm{I}} z}, \quad z \le 0$$
$$r'_n = \begin{cases} r_n - 1, & n = 1 \\ r_n, & n \neq 1 \end{cases}. \tag{3}$$

Note that r_n is the new nth reflection coefficient. The field in Region III, the output analytical region, is made of the transmitted waves scattered off the FD-FD region as

$$u^{\mathrm{III}}(x,z) = \sum_{n=1}^{N} t_n \phi_n^{\mathrm{III}}(x) e^{-j\beta_n^{\mathrm{III}}(z-L_z)}. \quad z > L_z \tag{4}$$

Here $\phi_n^{\mathrm{III}}(x)$ and β_n^{III} is the nth eigenmode and corresponding propagation constant of the exit waveguide while t_n is the nth transmission coefficient. For a parallel-plate waveguide filled with a homogeneous dielectric material, the eigenmodes $\{\phi_n(x)\}$ are simple sinusoidal functions. The normalized eigenfunction of a TE-polarized

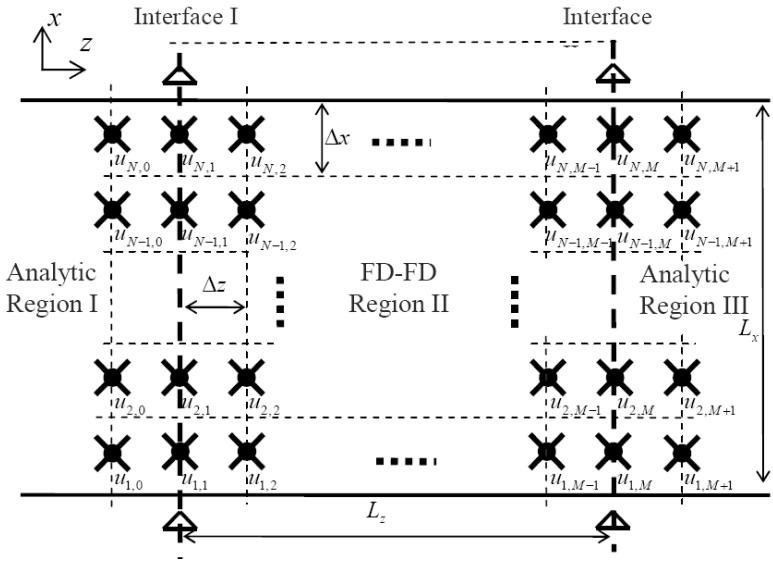

Figure 2. The Layout of the grid points in the FD-FD region shows a total of $N \times M$ unknowns in the L_z by L_x domain. The first and the last column of grid vectors are auxiliary variables located in the analytical regions.

field bounded by a pair perfectly electric conducting walls (PECWs) is given by

$$\phi_n(x) = \sqrt{\frac{2}{L_x}} \sin \frac{n\pi x}{L_x}, \quad \beta_n = \sqrt{k^2 - \left(\frac{n\pi}{L_x}\right)^2}, \quad n = 1, \ldots, N \tag{5}$$

The normalized eigenfunction of a TE-polarized field bounded by a pair perfectly magnetic conducting walls (PMCWs) is given by

$$\begin{aligned} \phi_n(x) &= \sqrt{\frac{\varepsilon_n}{L_x}} \cos \frac{n\pi x}{L_x}, \quad \varepsilon_n = \begin{cases} 1, & n = 0 \\ 2, & n \geq 1 \end{cases}, \\ \beta_n &= \sqrt{k^2 - \left(\frac{n\pi}{Lx}\right)^2}, \quad n = 0, \ldots, N-1 \end{aligned} \tag{6}$$

Eigenmodes of other more complex cases can be obtained by numerically solving for the mode characteristic functions [3].

2.2. FD Approximation of Helmholtz Equation

The $E_y(x, z)$ component of the TE case satisfies the following 2-D Helmholtz equation:

$$\frac{\partial^2 E_y}{\partial x^2} + \frac{\partial^2 E_y}{\partial z^2} + n^2(x, z) k_0^2 E_y = 0. \tag{7}$$

Using superscripts e, h for polarization and subscripts c, u, d, l, r to denote relative spatial relation, i.e., center, up, down, left and right, we then apply the second-order accurate FD approximation to the 2-D Helmholtz equation for a field point u_c. This leads to the five-point TE FD-FD formulae connecting the four neighboring points u_u, u_d, u_l, u_r.

$$\begin{aligned} & c_u^e u_u + c_d^e u_d + c_l^e u_l + c_r^e u_r + c_c^e u_c = 0, \\ & c_u^e = c_d^e = \frac{1}{\Delta x^2}, \quad c_l^e = c_r^e = \frac{1}{\Delta z^2}, \\ & c_c^e = \overline{n^2} k_0^2 - (c_u^e + c_d^e + c_l^e + c_r^e). \end{aligned} \tag{8a}$$

If the field point u_c is located near by a material interface (as depicted by Figure 3), we must choose $\overline{n^2}$ as some "average" of $n^2(x, z)$ around the reference field point u_c. It is chosen to be the integration over rectangular box centered at the particular field point given below:

$$\overline{n^2} \triangleq \frac{1}{\Delta x \Delta z} \int_{z-\Delta z/2}^{z+\Delta z/2} \int_{x-\Delta x/2}^{x+\Delta x/2} n^2(x, z)\, dx\, dz. \tag{8b}$$

For the TM case, the $H_y(x,z)$ component satisfies the following 2-D Helmholtz equation:

$$\frac{\partial}{\partial x}\left[\frac{1}{n^2(x,z)}\frac{\partial}{\partial x}H_y\right]+\frac{\partial}{\partial z}\left[\frac{1}{n^2(x,z)}\frac{\partial}{\partial z}H_y\right]+k_0^2H_y(x,z)=0. \quad (9)$$

To derive TM FD coefficients near a material interface, we must take extra cares to ensure the continuity of tangential magnetic field and continuity of tangential electric field $E_t(x,z)$ which is related to $H_y(x,z)$ by

$$E_t(x,y)=\frac{1}{n^2(x,z)}\frac{\partial}{\partial n}H_y(x,y). \quad (10)$$

Some papers choose a local coordinate system consistent with the material interface [34, 35]. Local FD variables and FD coefficients are derived and used. They are related back to the global variables by interpolation. Such methods are suitable for material with large index contrasts. However, they produce complex anisotropic coefficients for both TE and TM cases, which make the coding very difficult. We propose to use a similar averaging scheme like the TE case for the TM coefficients. Consider the first term in Equation (9), using central difference approximation we have

$$\begin{aligned}&\frac{\partial}{\partial x}\left[\frac{1}{n^2(x,z)}\frac{\partial}{\partial x}H_y\right]\approx\frac{1}{\Delta x}\left[\frac{\mathrm{A}}{n^2(x+\Delta x/2,z)}-\frac{\mathrm{B}}{n^2(x-\Delta x/2,z)}\right]\\&\mathrm{A}=\left.\frac{\partial u_c}{\partial x}\right|_{x=x+\Delta x/2}\approx\frac{u_u-u_c}{\Delta x},\ \mathrm{B}=\left.\frac{\partial u_c}{\partial x}\right|_{x=x-\Delta x/2}\approx\frac{u_c-u_d}{\Delta x}.\end{aligned} \quad (11)$$

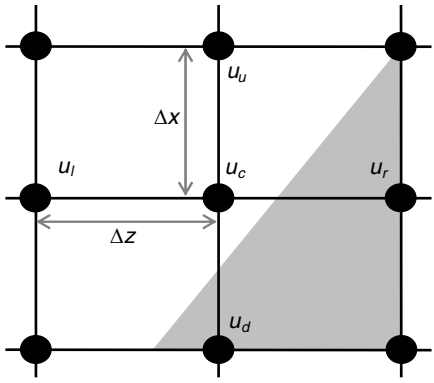

Figure 3. FD-FD TE grid points near a material interface.

Applying similar operation to the second term of Equation (9) we will obtain the following FD-FD coefficients for TM case:

$$\begin{aligned}
&\overline{\frac{1}{n_u^2}}\frac{u_u}{\Delta x^2}+\overline{\frac{1}{n_d^2}}\frac{u_d}{\Delta x^2}+\overline{\frac{1}{n_l^2}}\frac{u_l}{\Delta z^2}+\overline{\frac{1}{n_r^2}}\frac{u_r}{\Delta z^2}\\
&+\left(k_0^2-\left[\overline{\frac{1}{n_u^2}}+\overline{\frac{1}{n_d^2}}\right]\frac{1}{\Delta x^2}-\left[\overline{\frac{1}{n_l^2}}+\overline{\frac{1}{n_r^2}}\right]\frac{1}{\Delta z^2}\right)u_c=0,\\
&c_u^h u_u+c_d^h u_d+c_l^h u_l+c_r^h u_r+c_c^h u_c=0, \qquad (12a)\\
&c_u^h=\overline{\frac{1}{n_u^2}}\frac{1}{\Delta x^2},\ c_d^h=\overline{\frac{1}{n_d^2}}\frac{1}{\Delta x^2},\ c_l^h=\overline{\frac{1}{n_l^2}}\frac{1}{\Delta z^2},\ c_r^h=\overline{\frac{1}{n_r^2}}\frac{1}{\Delta z^2},\\
&c_c^h=k_0^2-\left(c_u^h+c_d^h+c_l^h+c_r^h\right).
\end{aligned}$$

Instead of using just one average as in the TE case, TM cases have four different averages for the up, down, left and right TM coefficients. The central coefficient c_c^h contains the term $c_u^h+c_d^h+c_l^h+c_r^h$ which is the sum of four neighboring coefficients. In addition, instead of the squared index as in the TE case, TM-integration is performed over the inverse of squared index given below:

$$\overline{\frac{1}{n^2}}\triangleq\frac{1}{\Delta x\,\Delta z}\int_{z-\Delta z/2}^{z+\Delta z/2}\int_{x-\Delta x/2}^{x+\Delta x/2}\frac{1}{n^2(x,z)}\,dx\,dz. \qquad (12b)$$

The integration domain is a rectangular box shifted half a grid up, down, left, right according to the subscript of the coefficient. Figure 4 further illustrates the four centers of integration in dotted circles.

The material-averaging formula for our FD-FD coefficients should reduce the well known "stair case effect" of plain FD methods. The detail error analysis on Equations (8a), (8b), (12a) and (12b) will be investigated in the near future.

2.3. Derivation of LM-TBC

So far we have derived FD-FD equation for all interior points in Region II. Points belong to $\mathbf{u}_1$ and $\mathbf{u}_M$ vectors are shared between the FD-FD region and the analytical regions. FD points on $\mathbf{u}_1$ are coupled to analytical points on $\mathbf{u}_0$. Also $\mathbf{u}_M$ vector is coupled to $\mathbf{u}_{M+1}$ vector. The fundamental idea of LM-TBC is that we can express, using the layer modes in each analytical region, $\mathbf{u}_0$ vector in term of $\mathbf{u}_1$ and $\mathbf{u}_{M+1}$ vectors in term of $\mathbf{u}_M$ via a full matrix.

Refer to Figure 2 we know that FD field points at Region I–II interface $z = 0$ can be computed from Equation (3) with the reflection coefficients as

$$u_{i,1} = u^{\mathrm{I}}(x_i, z = 0) = \sum_{n=1}^{N} r_n \phi_n^{\mathrm{I}}(x_i). \tag{13a}$$

Similarly we have

$$u_{i,0} = u^{\mathrm{I}}(x_i, -\Delta z) = 2j\phi_1^{\mathrm{I}}(x_i)\sin(\beta_1^{\mathrm{I}}\Delta z) + \sum_{n=1}^{N} r_n \phi_n^{\mathrm{I}}(x_i) e^{-j\beta_n^{\mathrm{I}}\Delta z} \tag{13b}$$

Let us define the eigenfunction matrix $\mathbf{\Phi}_{\mathrm{L}}$ and the propagation matrix $\mathbf{P}_{\mathrm{L}}$ for the input waveguide region as

$$\mathbf{\Phi}_{\mathrm{L}} \triangleq \left[\boldsymbol{\varphi}_1^{\mathrm{I}}, \boldsymbol{\varphi}_2^{\mathrm{I}}, \ldots, \boldsymbol{\varphi}_M^{\mathrm{I}}\right], \quad \boldsymbol{\varphi}_i^{I} \triangleq \begin{bmatrix} \phi_i^{\mathrm{I}}(x_1) \\ \phi_i^{\mathrm{I}}(x_2) \\ \vdots \\ \phi_i^{\mathrm{I}}(x_N) \end{bmatrix}, \tag{14a}$$

$$\mathbf{P}_{\mathrm{L}}(\Delta z) \triangleq \begin{bmatrix} e^{-j\beta_1^{\mathrm{I}}\Delta z} & \cdots & 0 \\ 0 & \ddots & 0 \\ 0 & \cdots & e^{-j\beta_N^{\mathrm{I}}\Delta z} \end{bmatrix}. \tag{14b}$$

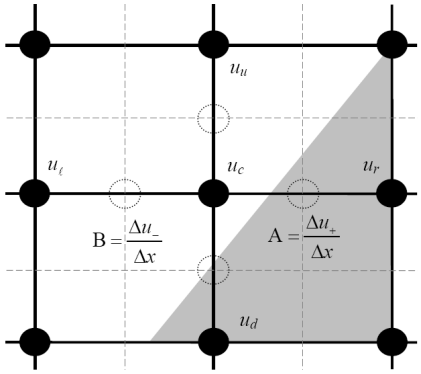

Figure 4. FD-FD TM grid points near a material interface. The four circled points are centers of integration for TM coefficients.

Then we have

$$\mathbf{u}_0 = \begin{bmatrix} u_{1,0} \\ \vdots \\ u_{N,0} \end{bmatrix} = 2j\sin(\beta_1^I \Delta z)\boldsymbol{\varphi}_1^I + \boldsymbol{\Phi}_{\mathrm{L}} \cdot \mathbf{P}(\Delta z) \cdot \mathbf{r}, \tag{15a}$$

where

$$\mathbf{r} \triangleq \begin{bmatrix} r_1 \\ r_2 \\ \vdots \\ r_N \end{bmatrix} = \boldsymbol{\Phi}_{\mathrm{L}}^{-1} \cdot \mathbf{u}_1. \tag{15b}$$

Finally we obtain the equation that relates $\mathbf{u}_0$ to $\mathbf{u}_1$ and the incident wave.

$$\mathbf{u}_0 = 2j\sin(\beta_1^{\mathrm{I}} \Delta z)\boldsymbol{\varphi}_1^{\mathrm{I}} + \mathbf{A}_{\mathrm{L}} \cdot \mathbf{u}_1, \quad \mathbf{A}_{\mathrm{L}} = \boldsymbol{\Phi}_{\mathrm{L}} \cdot \mathbf{P}_{\mathrm{L}}(\Delta z) \cdot \boldsymbol{\Phi}_{\mathrm{L}}^{-1}. \tag{16}$$

Note that $\boldsymbol{\Phi}_{\mathrm{L}}^{-1}$ can be approximated by the its own transpose $\boldsymbol{\Phi}_{\mathrm{L}}^{T}$ for real dielectric waveguide whose eigenfunctions are orthogonal to each other and can be normalized. To relate $\mathbf{u}_{M+1}$ to $\mathbf{u}_M$, we evaluate Equation (4) at $\mathbf{u}_M$ and $\mathbf{u}_{M+1}$ points. We have

$$u_{i,M} = u^{\mathrm{III}}(x_i, L_z) = \sum_{n=1}^{N} t_n \phi_n^{\mathrm{III}}(x_i), \tag{17a}$$

and

$$u_{i,M+1} = u^{\mathrm{III}}(x_i, L_z + \Delta z) = \sum_{n=1}^{N} t_n \phi_n^{\mathrm{III}}(x_i) e^{-j\beta_n^{\mathrm{III}} \Delta z}. \tag{17b}$$

$$\mathbf{t} = \begin{bmatrix} t_1 \\ t_2 \\ \vdots \\ t_N \end{bmatrix} = \boldsymbol{\Phi}_{\mathrm{R}}^{-1} \cdot \mathbf{u}_M. \tag{17c}$$

$$\mathbf{u}_{M+1} = \begin{bmatrix} u_{1,(M+1)} \\ \vdots \\ u_{N,(M+1)} \end{bmatrix} = \mathbf{A}_{\mathrm{R}} \cdot \mathbf{u}_M, \ \mathbf{A}_{\mathrm{R}} = \boldsymbol{\Phi}_{\mathrm{R}} \cdot \mathbf{P}_{\mathrm{R}}(\Delta z) \cdot \boldsymbol{\Phi}_{\mathrm{R}}^{-1}. \tag{17d}$$

Note that the eigenfunction matrix $\boldsymbol{\Phi}_{\mathrm{R}}$ and the propagation matrix $\mathbf{P}_{\mathrm{R}}$ in the exit waveguide region are defined by Equations (14a) and (14b) in a similar way.

2.4. Inverting the FD-FD Linear Equation

We now have FD-FD equations for all field points in the transition region. These variables are organized into M column vectors which satisfy a block tri-diagonal matrix equation with a bandwidth of $2N+1$. Since research on finding robust iterative methods for solving discretized Helmholtz equation is still being actively pursued, we turn to direct methods for the numerical solution of the banded matrix equation such as Gaussian elimination or the LU factorization. Both methods require about $N^3 \cdot M$ floating point operations. A modern day high-end PC with 4GB memory can hold up a quarter million variables, i.e., $N, M \approx 500$, and intermediate storage in core memory. The total run time for the largest problem is well under ten minutes.

3. FD-FD RESULTS AND VERIFICATION

To illustrate and verify numerical results computed by our proposed hybrid FD-FD method, we consider the following two problems, 1. two-dimensional (2-D) free space Green's function (FSGF), 2. 2-D Green's function of a dielectric slab waveguide (SWGF). The FD-FD results are compared with exact analytical solution or by the rigorous semi-analytical method.

3.1. Two-dimensional Free Space Green's Function

The Helmholtz equation for the two-D free space Green's function due to a line source located in the origin is given by [3]

$$\left(\nabla_t^2 + k_0^2\right) G\left(x, z\right) = -\delta(x)\delta(z). \tag{18a}$$

The analytic closed-form solution is in term of the Hankel function of the second kind as

$$G(\rho) = -\frac{j}{4} H_0^{(2)}(k_0\rho), \quad \rho = \sqrt{x^2 + z^2} \tag{18b}$$

In Figure 5 we compute and plot the 2-D field distribution the free-space Green's function computed by our hybrid FD-FD method and by using Equation (18b), the exact analytic expression. Due to symmetry in x and z we show only a rectangular slice using $N_x = 400$ by, $N_z = 80$ grids with the line source located at the lower right corner. For the hybrid FD-FD we set the discretization density $N_\lambda = 32$ which is number of points per wavelength so that $\Delta x = \Delta z = \lambda/N_\lambda$. We use LM-TBC for the left computational boundary and an even-symmetry

boundary condition for the right and bottom boundaries. Since all the N_z field points located on the top computational boundary are more than ten wavelengths away from the line source, we may approximate the field at $u_{N_x,k}$ by a local plane wave coming at an angle

$$\theta_k = \tan^{-1} \frac{k\Delta z}{N_x \Delta x}, \quad k = 0, 1, \ldots, N_z. \tag{19a}$$

Since $\theta_k \ll 1$, we use the following one-term TBC for grid points just above the top boundary:

$$u_{N_x+1,k} = u_{N_x,k} \cdot \exp\left(-jk_0 \cos\theta_k \Delta x\right). \tag{19b}$$

We see from comparing FD-FD images with those computed by the exact solution that both the one-term TBC and LM-TBC work very well.

To compute and quantify the FD-FD errors, we zero out the lower right 4 by 4 corner points to remove the field singularity. We also normalize the two complex field arrays so that the root mean square (RMS) value of each simulation is set to be one. The RMS error which

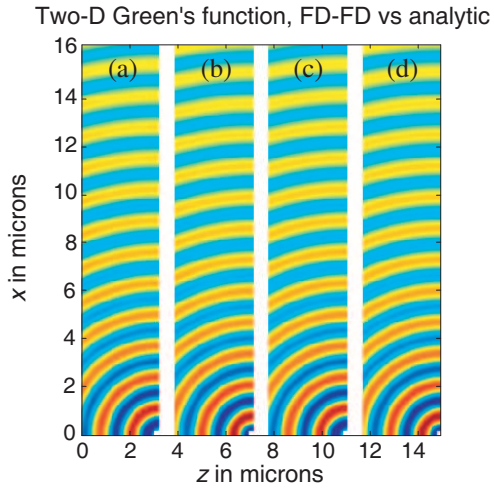

Figure 5. Real and imaginary part of the 2-D free space Green's function. The line source is located at the lower right corner. (a) FD-FD real, (b) FD-FD imaginary, (c) analytic real and (d) analytic imaginary.

is defined as

$$E_{\mathrm{RMS}}^{\mathrm{FD}} = \left\{ \frac{1}{(N_z+1)(N_x+1)} \sum_{k=0}^{N_z} \sum_{i=0}^{N_x} |u_{i,k} - u(x_i, z_k)|^2 \right\}^{1/2}, \quad (20)$$

where $\{u_{i,k}\}$ is the normalized complex FD-FD field and $u(x_i, z_k)$ is the normalized complex 2-D free-space Green's function. Using $N_\lambda = 32$, we compute $E_{\mathrm{RMS}}^{\mathrm{PMCW}} = 0.16$ for LM-TBC with a top PMCW and $E_{\mathrm{RMS}}^{\mathrm{PECW}} = 0.14$ for LM-TBC with a top PECW. We will show that the RMS error of the combined field $E_{\mathrm{RMS}}^{\mathrm{MW+EW}}$ is reduced to .053.

3.2. Reducing LM-TBC Corner Reflection

Even though we take very careful steps processing the four FD-FD computational edges, we are still seeing quite significant amount of reflected energy scattering off the top-left corner due to the upper PMCW in the LM-TBC region. It is known that the planar reflection coefficient from the PEMW changes sign when the wall is replaced by a PECW. To further reduce LM-TBC corner reflection all our hybrid FD-FD calculations in Figure 5 and all the remaining figures are computed as the average of the two independent FD-FD simulations each with an opposite wall type. In other words,

$$u_{i,j} = \frac{1}{2}\left(u_{i,j}^{\mathrm{PECW}} + u_{i,j}^{\mathrm{PMCW}}\right), \quad \text{for all} \quad i, j. \quad (21)$$

This would help to cancel some but not all reflected power. The new $E_{\mathrm{RMS}}^{\mathrm{MW+EW}}$ is now reduced to .053 which is not much larger than the expected phase error produced by the standard five-point FD approximation to the continuous Laplacian operator. The difference between the two calculations along the LM-TBC boundary is plotted on the top of Figure 6 along with the line plot of the exact 2-D Green's function (GF). The RMS of absolute errors for this trace is 0.072. For comparison, the same RMS errors for the trace passes through the line source is 0.029. We see that LM-TBC has done its job and produces small difference from the exact solution. We also notice that the error is greater near the corner where the two TBC boundaries meet.

3.3. Two-dimensional Green's Function in an Open Dielectric Slab Waveguide

To verify LM-TBC's performance in a layer structure, we plot in Figure 7, 2-D TE $E_y(x, z)$ field distribution of slab waveguide Green's

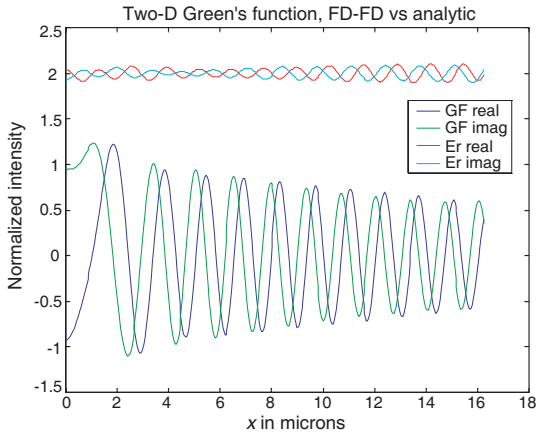

Figure 6. Real and imaginary part of the 2-D free space Green's function along the LM-TBC boundary. The top two curves are the difference between the two methods. For clarity, an offset is added to the dc-free error traces. The RMS of the absolute errors is 0.072.

function computed by our hybrid FD-FD method and by the following semi-analytical expression [36]:

$$G\left(x,z\right)=\sum_{n=1}^{\infty}g_n\left(z\right)\phi_n\left(x\right)=\sum_{n=1}^{\infty}\frac{\phi_n\left(0\right)}{2j\beta_n}\phi_n\left(x\right)e^{-j\beta_n|z|},$$

$$\delta(x)=\sum_{n=1}^{\infty}\phi_n\left(0\right)\phi_n\left(x\right), \tag{22}$$

$$\left(\frac{d^2}{dz^2}+\beta^2\right)g_n\left(z\right)=-\delta\left(z\right),\quad g_n\left(z\right)=\frac{1}{2j\beta_n}e^{-j\beta_n|z|}.$$

Here ϕ_n is the nth discretized slab waveguide mode function. Like the LM-TBC formulation, $G(x,z)$ in Equation (22) is the line source response of a dielectric slab waveguide confined inside a pair of parallel walls. Vertically traveling EM waves can not escape from the two parallel walls. In the limit of an infinite wall separation, $G(x,z)$ becomes the exact unbounded Green's function. To ensure that we are computing accurate semi-analytical solutions, the PECW and PMCW are placed at $L_x = 1950\,\mu$m far away from the core. The reference semi-analytical solutions are taken from the average of two calculations:

$$u(x,z)=\frac{1}{2}\Big(u^{\mathrm{PECW}}(x,z)+u^{\mathrm{PMCW}}(x,z)\Big). \tag{23}$$

The slab waveguide is made of a 0.8 μm thick glass core surrounded in the air operated at $\lambda = 1.3\,\mu$m. We use the same $N_x = 400$ by $N_z = 80$ FD-FD grid size with the line source located at the lower right corner. Core grid density is set at $N_\lambda = 32$ making $N_\lambda = 48$ for grid points in the air. The same one-term TBC is used for up most grid points located at $x = 10.4\,\mu$m. The incident ray angles are computed from the primary arriving rays under geometry optics and Snell's law. The TM $H_y(x, z)$ results are plotted in Figure 8.

Compared with reference semi-analytical solutions, we observe $E^{\text{TE}}_{\text{RMS}} = 0.073$ and $E^{\text{TM}}_{\text{RMS}} = 0.056$ for our hybrid FD-FD method. The errors are slightly higher than the free space case. We believe that some part of the errors is from the effects of finite PECW/PMCW separation, some comes from the simple one-term TBC at the top boundary. To save space, we will not repeat line plots of absolute differences considering also that the error distribution in Figures 7 and 8 for the slab waveguide are similar to those in the free space case.

We see from Equation (22) that the line source excites various

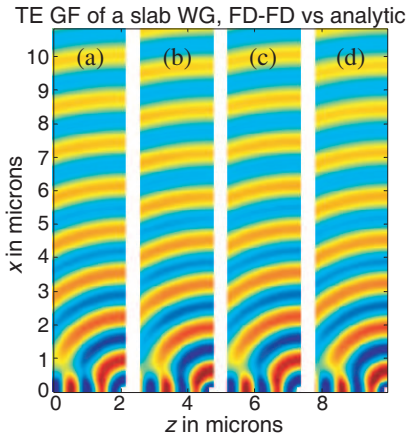

Figure 7. Real and imaginary part of the 2-D TE field in an open slab waveguide due to a line source at the lower right corner. (a) FD-FD real, (b) FD-FD imaginary, (c) analytic real, (d) analytic imaginary.

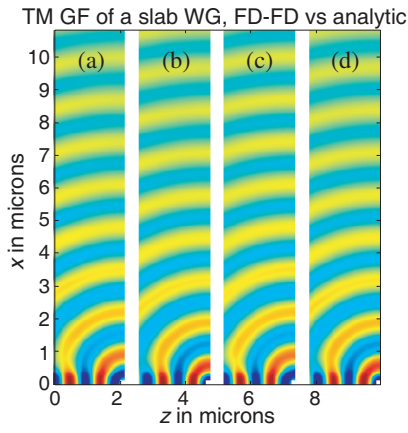

Figure 8. Real and imaginary part of the 2-D TM field in an open slab waveguide due to a line source at the lower right corner. (a) FD-FD real, (b) FD-FD imaginary, (c) analytic real and (d) analytic imaginary. All the parameters except the polarization are the same as those in Figure 7.

modes in the slab waveguide. These mode fields are clearly transmitted off the FD domain as there are visually no difference between the FD and the semi-analytical simulations. Thus, except near the FD corners, LM-TBC is capable of absorbing/transmitting all modes including guiding modes, cladding modes and even evanescent waves across the FD-Analytic domain junction. We also notice from comparing Figure 7 with Figure 8 that TM wave fields are better confined in the waveguide than the TE wave fields.

Our final numerical verification is the study of scattered power in the quasi-adiabatic linear tapered waveguide example of Figure 1. The taper slope is increased to 30 degrees in order to produce enough reflection to justify the use of bi-directional full-wave algorithm of our hybrid FD-FD method. We also use a higher grid density with $N_\lambda = 30/45$ in the core/cladding region to reduce FD-FD grid dispersion error. Our hybrid FD-FD method will be compared with a semi-analytical method called couple transverse-mode integral-equation (CTMIE) [37]. The tapered waveguide is "stair-case" approximated using 51 slices of slab waveguides. From these slice modes (720 for each slice), CTMIE constructs the integral operators and computes the normalized reflected and transmitted powers of the tapered waveguide. The power coefficients are further divided into guided power and

Table 1. Comparison of computed power reflection and transmission coefficients of a 30 degree linear taper waveguide from a 4.65 μm thick input slab waveguide to a 2 μm thick output slab waveguide. The capital letter G/R denotes guided/radiating power and lower case letter r/t stands for reflected/transmitted power. Other parameters are the same as in Figure 1.

	Polarization	CTMIE 51 slices	FDFD $N_\lambda = 30$
G_r	TE	0.0009	0.0010
	TM	0.0005	0.0004
G_t	TE	0.8258	0.8252
	TM	0.8471	0.8493
R_r	TE	0.0016	0.0012
	TM	0.0020	0.0022
R_t	TE	0.1716	0.1714
	TM	0.1504	0.1518

radiating power ratios. Both TE and TM polarization are compared and the numerical results are listed in Table 1.

Although the relative errors in reflected power G_r and R_r are more than 10 percents, the absolute values are very small. The much larger transmitted powers G_t and G_r agree with each other with a better than 99% accuracy. As a result, we are confident that both methods produce valid answers. Thus, the proposed hybrid FD-FD method is suitable for studying complex, small to medium size, optical waveguide devices.

While LM-TBC is developed for the 2-D hybrid FDFD method, the boundary condition could be of interest to those FDTD researchers who are interested in novel boundary conditions. It can be modified as a convolution operator to work with FDTD methods in 2D and 3D applications.

4. CONCLUSION

In this paper, we develop a hybrid FD-FD method suitable for studying two-dimensional optical waveguide devices for both TE and TM polarizations. Our layer-mode based transparent boundary condition, LM-TBC, is capable of launching an incident wave and simultaneously, directing the reflected and the transmitted scattered wave fields back and forward to the analytical regions. Using the exact free space Green's function, an "approximate" Green's function for a dielectric slab waveguide and a semi-analytic solution to a linearly tapered waveguide, we verify the effectiveness of our propose hybrid FD-FD method which allows us to solve for many complex 2-D waveguide devices with horizontally stratified input/output waveguides.

ACKNOWLEDGMENT

We are grateful to the support of the National Science Council of the Republic of China under the contracts NSC97-972221-E-110016. This work is also supported by the Ministry of Education, Taiwan, under the Aim-for-the-Top University Plan.

REFERENCES

1. Lin, C. F., *Optical Components for Communications*, Kluwer Academic Publishing, Boston, 2004.
2. Pavesi, L. and G. Guillot, *Optical Interconnects, the Silicon Approach*, Springer-Verlag, Berlin, 2006.

3. Ishimaru, A., *Electromagnetic Propagation, Radiation, and Scattering*, Prentice Hall, Englewood Clifffs, N.J., 1991.
4. Chew, W.-C., *Waves and Fields in Inhomogeneous Media*, Van Norstrand Reinhold, New York, 1990.
5. Taflove, A. and S. Hagness, *Computational Electrodynamics: The Finite-difference Time-domain Method*, Artech House, Norwood, MA, 2000.
6. Zheng, G., A. A. Kishk, A. W. Glisson, and A. B. Yakovlev, "A novel implementation of modified Maxwell's equations in the periodic finite-difference time-domain method," *Progress In Electromagnetics Research*, PIER 59, 85–100, 2006.
7. Shao, W., S.-J. Lai, and T.-Z. Huang, "Compact 2-D full-wave order-marching time-domain method with a memory-reduced technique," *Progress In Electromagnetics Research Letters*, Vol. 6, 157–164, 2009.
8. Yamauchi, J., *Propagating Beam Analysis of Optical Waveguides*, Research Studies Press, Baldock, England, 2003.
9. Yee, K. S., "Numerical solution of initial boundary value problems involving Maxwell's equations in isotropic media," *IEEE Trans. Antennas and Propagation*, Vol. 14, 302–307, 1966.
10. Taflove, A. and M. Brodwin, "Numerical solution of steady-state electromagnetic scattering problem using the time-dependent Maxwell's equations," *IEEE Trans. Microwave Theory and Techniques*, Vol. 23, 623–630, 1975.
11. Taflove, A. and M. Brodwin, "Computation of the electromagnetic fields and induced temperatures within a model of the microwave-irradiated human eye," *IEEE Trans. Microwave Theory and Techniques*, Vol. 23, 888–896, 1975.
12. Holland, R., "Threde: A free-field EMP coupling and scattering code," *IEEE Trans. Nuclear Science*, Vol. 24, 2416–2421, 1977.
13. Kunz, K. S. and K. M. Lee, "A three-dimensional finite-difference solution of the external response of an aircraft to a complex transient EM environment 1: The method and its implementation," *IEEE Trans. Electromagnetic Compatibility*, Vol. 20, 328–333, 1978.
14. Huang, Y. C., "Study of absorbing boundary conditions for finite difference time domain simulation of wave equations," Master Thesis, Graduate Institute of Communication Engineering, National Taiwan University, June 2003.
15. Mur, G., "Absorbing boundary conditions for the finite difference approximation of the time domain electromagnetic field equation,"

IEEE Trans. Electromagnetic Compat. EMC-23, Vol. 4, 377–382, 1981.

16. Lindman, E. L., "Free-space boundary conditions for the time dependent wave equation," *J. Comp. Phys.*, Vol. 18, 66–78, 1975.
17. Liao, Z. P., H. Wong, B. Yang, and Y. F. Yuan, "A transmitting boundary for transient wave analysis," *Scientia Sinica (Series A)*, Vol. 27, 1063–1076, 1984.
18. Grote, M. and J. Keller, "Nonreflecting boundary conditions for time dependent scattering," *J. Comp. Phys.*, Vol. 127, 52–81, 1996.
19. Engquist, B. and A. Majda, "Absorbing boundary conditions for the numerical simulation of waves," *Math Comp.*, Vol. 31, 629–651, 1971.
20. Engquist, B. and A. Majda, "Radiation boundary conditions for acoustic and elastic wave calculations," *J. Comp. Phys.*, Vol. 127, 52–81, 1996.
21. Hadley, G. R., "Transparent boundary conditions for the beam propagation method," *IEEE J. Quantum Electron*, Vol. 28, 363–370, 1992.
22. Berenger, J. P., "A perfectly matched layer for the absorption of electromagnetic waves," *J. Comp. Phys.*, Vol. 114, 185–200, 1994.
23. Berenger, J. P., "Perfectly matched layer for the FDTD solution of wave-structure interaction problems," *IEEE Trans. Antennas and Propagation*, Vol. 44, No. 1. 110–117, 1996.
24. Zheng, K., W.-Y. Tam, D.-B. Ge, and J.-D. Xu, "Uniaxial PML absorbing boundary condition for truncating the boundary of dng metamaterials," *Progress In Electromagnetics Research Letters*, Vol. 8, 125–134, 2009.
25. Juntunen, J. S., "Zero reflection coefficient in discretized PML," *IEEE Microwave and Wireless Compt. Letter*, Vol. 11, No. 4, 2001.
26. Johnson, S. G., "Notes on perfectly matched layers (PMLs), MIT 18.369 and 18.336 course note, July 2008.
27. Hwang, J.-N., "A compact 2-D FDFD method for modeling microstrip structures with nonuniform grids and perfectly matched layer," *Trans. on MTT.*, Vol. 53, 653-659, Feb. 2005.
28. Robertson, M. J., S. Ritchie, and P. Dayan, "Semiconductor waveguides: Analysis of optical propagation in single rib structures and directional couplers," *Inst. Elec. Eng. Proc.-J.*, Vol. 132, 336–342, 1985.
29. Vassallo, C., "Improvement of finite difference methods for step-index optical waveguides," *Inst. Elec. Eng. Proc.-J.*, Vol. 139, 137–

142, 1992.

30. Hua, Y., Q. Z. Liu, Y. L. Zou, and L. Sun, "A hybrid FE-BI method for EM scattering from dielectric bodies partiallycovered by conductors," *Journal of Electromagnetic Waves and Applications*, Vol. 22, No. 2–3, 423–430, 2008.
31. Wang, S.-M., "Development of large-scale FDFD method for passive optical devices," Master Thesis (in Chinese), Institute of Elctro-Optical Engineering, National Sun Yat-sen University, June 2005.
32. Chang, H. W. and W. C. Cheng, "Analysis of dielectric waveguide termination with tilted facets by analytic continuity method," *Journal of Electromagnetic Waves and Applications*, Vol. 21, No. 12, 1653–1662, 2007.
33. Cheng, W.-C. and H.-W. Chang, "Comparison of PML with layer-mode based TBC for FD-FD method in a layered medium," *International Conference on Optics and Photonics in Taiwan*, P1-170, Dec. 2008.
34. Chiang, Y. C., Y. Chiou, and H. C. Chang, "Improved full-vectorial finite-difference mode solver for optical waveguides with step-index profiles," *J. of Lightwave Technology*, Vol. 20, No. 8, 1609–1618, August 2002.
35. Lavranos, C. S. and G. Kyriacou, "Eigenvalue analysis of curved waveguides employing an orthogonal curvilinear frequency domain finite difference method," *IEEE Microwave Theory and Techniques*, Vol. 57, 594–611, March 2009.
36. Magnanini, R. and F. Santosa, "Wave propagation in a 2-D optical waveguide," *SIAM J. Appl. Math.*, Vol. 61, No. 4. 1237–1252, 2000.
37. Chang, H.-W. and M.-H. Sheng, "Field analysis of dielectric waveguide devices based on coupled transverse-mode integral equation — Mathematical and numerical formulations," *Progress In Electromagnetics Research*, PIER 78, 329–347, 2008.